



## Probing the role of chloride in Photosystem II from *Thermosynechococcus elongatus* by exchanging chloride for iodide

Alain Boussac<sup>a,\*</sup>, Naoko Ishida<sup>a</sup>, Miwa Sugiura<sup>b,c</sup>, Fabrice Rappaport<sup>d</sup>

<sup>a</sup> iBiTec-S, CNRS UMR 8221, CEA Saclay, 91191 Gif-sur-Yvette, France

<sup>b</sup> Cell-Free Science and Technology Research Center, Ehime University, Bunkyo-cho, Matsuyama Ehime, 790–8577, Japan, and PRESTO, Japan Science and Technology Agency (JST), 4-1-8, Honcho, Kawauchi, Saitama 332–0012, Japan

<sup>c</sup> Department of Chemistry, Graduate School of Science and Technology, Ehime University, Bunkyo-cho, Matsuyama, Ehime 790–8577, Japan

<sup>d</sup> Institut de Biologie Physico-Chimique, UMR 7141 CNRS and Université Pierre et Marie Curie, 13 rue Pierre et Marie Curie, 75005 Paris, France

### ARTICLE INFO

#### Article history:

Received 19 January 2012

Received in revised form 21 February 2012

Accepted 24 February 2012

Available online 1 March 2012

#### Keywords:

Photosystem II

Chloride

Oxygen evolution

### ABSTRACT

The active site for water oxidation in Photosystem II (PSII) goes through five sequential oxidation states ( $S_0$  to  $S_4$ ) before  $O_2$  is evolved. It consists of a  $Mn_4CaO_5$  cluster and Tyr<sub>Z</sub>, a redox-active tyrosine residue. Chloride ions have been known for long time to be required for the function of the enzyme. However, X-ray data have shown that they are located about 7 Å away from the  $Mn_4CaO_5$  cluster, a distance that seems too large to be compatible with a direct involvement of chloride in the water splitting chemistry. We have investigated the role of this anion by substituting  $I^-$  for  $Cl^-$  in the cyanobacterium *Thermosynechococcus elongatus* with either  $Ca^{2+}$  or  $Sr^{2+}$  biosynthetically assembled into the  $Mn_4$  cluster. The electron transfer steps affected by the exchanges were investigated by time-resolved UV–visible absorption spectroscopy, time-resolved EPR at room temperature and low temperature cw-EPR spectroscopy. In both Ca-PSII and Sr-PSII, the  $Cl^-/I^-$  exchange considerably slowed down the two  $S_3Tyr_Z^* \rightarrow (S_3Tyr_Z^*)' \rightarrow S_0$  reactions in which the fast phase,  $S_3Tyr_Z^* \rightarrow (S_3Tyr_Z^*)'$ , reflects the electrostatically triggered expulsion of one proton from the catalytic center caused by the positive charge near/on Tyr<sub>Z</sub><sup>\*</sup> and the slow phase corresponds to the  $S_0$  and  $O_2$  formations and to a second proton release. The  $t_{1/2}$  for  $S_0$  formation increased from 1.1 ms in Ca/Cl-PSII to  $\approx 6$  ms in Ca/I-PSII and from 4.8 ms in Sr/Cl-PSII to  $\approx 45$  ms in Sr/I-PSII. In all cases the Tyr<sub>Z</sub><sup>\*</sup> reduction was the limiting step. The kinetic effects are interpreted by a model in which the  $Ca^{2+}$  binding site and the  $Cl^-$  binding site, although spatially distant, interact. This interaction is likely mediated by the H-bond and/or water molecules network(s) connecting the  $Cl^-$  and  $Ca^{2+}$  binding sites by which proton release may be channelled.

© 2012 Elsevier B.V. All rights reserved.

### 1. Introduction

Light-driven water oxidation catalyzed by Photosystem II (PSII) is the first step in the photosynthetic production of biomass, fossil fuels and  $O_2$  on Earth. Refined three dimensional X-ray structures from 3.5 Å to 2.9 Å resolution have been obtained with PSII isolated from the thermophilic cyanobacterium *Thermosynechococcus elongatus* [1,2]. An X-ray structure with a 1.9 Å resolution, obtained using PSII isolated from the thermophilic cyanobacterium *Thermosynechococcus vulcanus*, has been described recently [3]. PSII is made up of 17

transmembrane protein subunits, 3 extrinsic proteins. Altogether these bear 35 chlorophyll, 2 pheophytins, 2 hemes, 1 non-heme iron, 2 quinones, 3–4 calcium ions, one of which in the  $Mn_4CaO_5$  cluster, 3 chloride ions, among these three only two are in the vicinity of the  $Mn_4CaO_5$  and located respectively  $\approx 6.7$  Å (site 1) and  $\approx 7.4$  Å (site 2) apart from the  $Mn_4CaO_5$ , 11–12 carotenoid molecules, more than 20 lipids and more than 1300 water molecules [3].

The exciton resulting from the absorption of a photon by the antennae is transferred to the photochemical trap which undergoes a charge separation. The positive charge is then stabilized on  $P_{680}$ , a weakly coupled chlorophyll dimer ( $P_{D1}$  and  $P_{D2}$ ). Then,  $P_{680}^{+\bullet}$  oxidizes a tyrosine residue of the D1 polypeptide, Tyr<sub>Z</sub>, which in turn oxidizes the  $Mn_4CaO_5$  cluster. On the acceptor side, the pheophytin anion ( $Pheo_{D1}^-$ ) transfers the electron to the primary quinone electron acceptor,  $Q_A$ , which in turn reduces a second quinone,  $Q_B$ .  $Q_A$  is tightly bound and acts as a one-electron carrier whereas  $Q_B$  acts as a two-electron and two-proton acceptor with a stable semiquinone intermediate,  $Q_B^{\bullet-}$ . While the  $Q_B^{\bullet-}$  semiquinone state is tightly bound, its quinone and quinol forms are exchangeable with the quinone pool in the thylakoid membrane, e.g. [4–10].

**Abbreviations:** PSII, Photosystem II; Chl, chlorophyll; PPBQ, phenyl-*p*-benzoquinone; MES, 2-(*N*-morpholino) ethanesulfonic acid;  $P_{680}$ , chlorophyll dimer acting as the second electron donor;  $Q_A$ , primary quinone acceptor;  $Q_B$ , secondary quinone acceptor; 43H, *T. elongatus* strain with a His-tag on the C terminus of CP43; EPR, Electron Paramagnetic Resonance; PQ, plastoquinone 9; WT\*1, WT\*2, WT\*3, mutant *T. elongatus* cells expressing only the *psbA1*, *psbA2*, *psbA3* gene, respectively;  $Pheo_{D1}$ , pheophytin;  $P_{D1}$  and  $P_{D2}$ , Chl monomer of  $P_{680}$  on the D1 or D2 side, respectively

\* Corresponding author. Tel.: +33 1 69 08 72 06; fax: 33 1 69 08 87 17.

E-mail address: [alain.boussac@cea.fr](mailto:alain.boussac@cea.fr) (A. Boussac).

The  $\text{Mn}_4\text{CaO}_5$  cluster accumulates oxidizing equivalents and is the catalytic site for water oxidation. The enzyme cycles sequentially through five redox states, denoted  $S_n$  where  $n$  stands for the number of stored oxidizing equivalents. Upon formation of the  $S_4$  state two molecules of water are rapidly oxidized, the  $S_0$  state is regenerated and  $\text{O}_2$  released [11,12].

The knowledge of the 3D structure has led to the computer assisted identification of channels compatible in diameter and physico-chemical properties with the conduction of water molecules [2,13–15]. The progress due to the 1.9 Å resolution of the crystallographic data [3] has allowed the identification of many water molecules with, even more importantly, some of which being arranged in rows forming water channels. Still, the water oxidation mechanism is far from being fully understood. This is mainly due to the lack of identified reaction intermediates in the  $S_3\text{Tyr}_Z^* + 2\text{H}_2\text{O} \rightarrow S_0 + \text{O}_2$  transition. Indeed, they have escaped detection so far mainly owing to the fact that the reduction of  $\text{Tyr}_Z^*$  is the limiting step of the overall water oxidation in the native enzyme.

DFT and QM/MM calculations, based on the previous PSII [1,2] or more recent structures [3] have proposed plausible water oxidation mechanisms with energetically favorable structures for the  $S_n$  states models [16–19] allowing the  $\text{O}=\text{O}$  bond formation. Most recent theoretical approaches benefitted from the knowledge of the water molecules positions in general. More specifically, they could integrate in the models the two water molecules bound to the calcium ion and the two others bound to the manganese ion protruding from the distorted cubane part of the  $\text{Mn}_4\text{CaO}_5$  cluster [18–20]. Each of the two water molecules bound to  $\text{Ca}^{2+}$  makes, directly or not, a H bond with  $\text{Tyr}_Z$ . The water molecules bound to the  $\text{Ca}^{2+}$  and to the manganese could thus simply fill the coordination sphere of these ions and would thus have merely a structural role. Alternatively, they may provide one or even two of the substrate water molecule(s) required to make the dioxygen.

The role of chloride has, until now e.g. [21–39], been mostly investigated in plant PSII in which  $\text{Cl}^-$  depletion results in the inhibition of oxygen evolution and perturbs the  $\text{Mn}_4\text{CaO}_5$ -cluster to a variable extent depending on the method used to extract  $\text{Cl}^-$ . Upon incubation in  $\text{Cl}^-$ -free buffer (or dialysis) the enzyme is functional, although at a reduced rate [26,32]. High pH values favour the  $\text{Cl}^-$ -depletion in  $\text{Cl}^-$ -free buffer [37,38]. In the presence of  $\text{SO}_4^{2-}$ , the EPR  $S_2$  multiline signal is no longer detectable [22] and the enzyme is blocked after the formation of the  $S_2\text{Tyr}_Z^*$  state [23]. In the  $\text{SO}_4^{2-}$ -treated enzyme the electron donation rate from  $\text{Tyr}_Z$  to  $\text{P}_{680}^{+\bullet}$  mainly occurred in the sub-microsecond time range in  $S_1$  and  $S_2$  [23] but incrementing the  $S$  states cycle from  $S_2$  to  $S_3$  and from  $S_3$  to  $S_0$  requires  $\text{Cl}^-$  [23,27]. The dependence of the consequences of  $\text{Cl}^-$ -depletion upon the method used to achieve it has been explained by the existence of more than one chloride-binding site in PSII with different affinities for  $\text{Cl}^-$ . The activity of PSII would be mainly controlled by the binding to the high affinity site and the activity of PSII is further modulated by the occupancy of the other, low affinity, site [25,26]. The existence of two  $\text{Cl}^-$  binding sites has been confirmed by structural data [3], see also [40,41].

Upon  $\text{Cl}^-$ -depletion the enzyme is blocked in a  $S_2\text{Tyr}_Z^*$  state characterized by a split EPR signal [23,25] reminiscent of that detected in  $\text{Ca}^{2+}$ -depleted PSII [42–44]. Yet, the similarity between  $\text{Ca}^{2+}$  and  $\text{Cl}^-$  depletions does not go much beyond this. Indeed, whereas the 1.9 Å resolution structure points to possible scenarios involving  $\text{Ca}^{2+}$  in the water oxidation mechanism, e.g. [17–19], rationalizing the involvement of  $\text{Cl}^-$  in the water oxidizing process on structural basis is far less straightforward. The distances between the  $\text{Mn}_4\text{CaO}_5$  cluster and the two  $\text{Cl}^-$  ions ( $\approx 7$  Å, at least in the  $S_n$  state corresponding to the structure [3]) seem to argue against a direct role for  $\text{Cl}^-$  in the water oxidation mechanism. Several possible roles have been put forward such as *i*) the tuning of the coordination sphere of the  $\text{Mn}_4\text{CaO}_5$  cluster via the D1–Glu333 and CP43–Glu354 each of these amino acids

belonging to the coordination sphere of both the  $\text{Mn}_4\text{CaO}_5$  cluster and one of the chloride ions [3] and *ii*) a role in the proton exit pathway, e.g. [3,21,23,32,45]. The later hypothesis was supported by a theoretical study according to which chloride depletion would induce the formation of a salt bridge between D2–Lys317 and D1–Asp61 that would impair the transfer of protons to the lumen [46].

One way to get insights into the role of the  $\text{Cl}^-$  cofactor is the use of surrogate ions, mainly  $\text{Br}^-$  and  $\text{I}^-$ . The efficiency of  $\text{I}^-$  as a substitute for  $\text{Cl}^-$  has been shown in plant PSII, at low  $\text{I}^-$  concentration [33]. In these conditions, the activity of  $\text{Cl}^-$ -depleted  $\text{I}^-$ -reconstituted PSII reached up to 70–80% of that measured in  $\text{Cl}^-$ -reconstituted PSII. Under flash illumination the miss parameter was found slightly larger and the  $t_{1/2}$  of the  $S_3\text{Tyr}_Z^* + 2\text{H}_2\text{O} \rightarrow S_0 + \text{O}_2$  transition slower ( $\approx 8$  ms instead of  $\approx 2$  ms) [34]. At high concentration,  $\text{I}^-$  has been shown to directly reduce the  $\text{Mn}_4\text{CaO}_5$  cluster [33] resulting in an increased rate for deactivation of the  $S_2$ -state and  $S_3$ -state [34]. With a high  $\text{I}^-$  concentration, labelling of PSII proteins has also been observed [47,48]. However, the exogenous reduction of the  $\text{Mn}_4\text{CaO}_5$  cluster is not mediated by the  $\text{I}^-$  ion that reactivates, likely by its binding to the  $\text{Cl}^-$  site, the  $\text{O}_2$  activity of  $\text{Cl}^-$ -depleted PSII [33]. Similarly, in PSII from *T. vulcanus*  $\text{Cl}^-/\text{I}^-$  exchange restores  $\text{O}_2$  evolving activity up to 1 mM  $\text{I}^-$  but inhibits oxygen evolution at higher concentrations [41]. Last, the  $\text{I}^-$  binding sites have been shown to correspond to the two  $\text{Cl}^-$  binding sites identified in the 1.9 Å resolution structure [3,41].

To get new insights into the role of chloride in the water oxidation mechanism we have studied the role of  $\text{Cl}^-/\text{I}^-$  replacement using PSII from the cyanobacterium *T. elongatus* with either  $\text{Ca}^{2+}$  or  $\text{Sr}^{2+}$  biosynthetically integrated into the  $\text{Mn}_4$  cluster [49–51]. The Ca/I-PSII and Sr/I-PSII were analyzed by using EPR spectroscopy and UV-visible time resolved absorption change spectroscopy.

## 2. Materials and methods

The *T. elongatus* strain used was a  $\Delta\text{psbA}_1\Delta\text{psbA}_2$  deletion mutant (WT\*3) [52] constructed from the *T. elongatus* 43-H strain that had a His<sub>6</sub>-tag on the C-terminus of CP43 [53]. PsbA3-PSII purified from WT\*3 cells has been used in the present study because this is the best characterized material for the  $\text{Ca}^{2+}$  and  $\text{Cl}^-$  exchange experiments, e.g. [49,54,55]. PSII were purified with the protocol already described [49]. The Ca/Sr exchange was done biosynthetically as previously described [49]. For the  $\text{Cl}^-/\text{I}^-$  exchange, Ca/Cl-PSII and Sr/Cl-PSII bound to the Ni-column were washed overnight with approximately 8–10 column volumes of a buffer containing 10% glycerol, 1 M betaine, 100 mM NaCl, 15 mM  $\text{CaCl}_2$ , 15 mM,  $\text{MgCl}_2$ , 40 mM MES, 1 mM L-histidine, 0.03%  $\beta$ -dodecyl maltoside, pH 6.5 (pH adjusted with NaOH). Then, the PSII samples bound to the resin were washed with one volume of resin with a buffer containing 10% glycerol, 1 M betaine, 1 mM NaI, 15 mM  $\text{Ca}(\text{OH})_2$ , 15 mM  $\text{Mg}(\text{OH})_2$ , 1 mM L-histidine, 0.03%  $\beta$ -dodecyl maltoside, MES 40 mM, pH 6.5 (adjusted by addition of NaOH). The PSII was then eluted with a buffer with 10% glycerol, 1 M betaine, 1 mM NaI, 15 mM  $\text{Ca}(\text{OH})_2$ , 15 mM  $\text{Mg}(\text{OH})_2$ , 200 mM L-histidine, 0.03%  $\beta$ -dodecyl maltoside, pH 6.5 (adjusted by addition of MES powder). The eluted PSII samples were then washed by using Amincon-ultra-15 100 K concentrators in a buffer containing 10% glycerol, 1 M betaine, 1 mM NaI, 15 mM  $\text{Ca}(\text{OH})_2$ , 15 mM  $\text{Mg}(\text{OH})_2$ , 40 mM MES 40 mM, pH 6.5 (pH adjusted with NaOH).

As mentioned earlier for Plant PSII, e.g. [26,32,36], and for PSII from *T. vulcanus* [41] the washing of *T. elongatus* PSII in a  $\text{Cl}^-$ -free medium resulted in only  $\approx 20\%$  inhibition of  $\text{O}_2$  evolution. The remaining activity close to 80% of the starting activity was interpreted, e.g. [41], as arising from  $\text{Cl}^-$  contaminations in the media used. Nevertheless, this  $\text{Cl}^-$  contamination did not prevent neither  $\text{Br}^-$ -reconstitution [40,41] nor  $\text{I}^-$ -reconstitution [41] from occurring since  $\text{Br}^-$  and  $\text{I}^-$  were clearly identified in the halide binding sites by X-ray

spectroscopy. Taking into account earlier studies [33] showing that due to the redox properties of  $I^-$  a too high concentration resulted in a loss of  $O_2$  evolution, the optimization of the  $Cl^-/I^-$  exchange protocol in PSII from *T. elongatus* and described earlier was done as follows. Both the duration of the incubation in  $I^-$ -containing media and the concentration of  $I^-$  were varied and the optimized conditions were deduced from 4 independent measurements. The kinetics of the  $S_3Tyr_z^* + 2H_2O \rightarrow S_0Tyr_z + O_2$  reaction was estimated first with a rate  $O_2$  electrode [49] and secondly by following the decay of the absorption at 292 nm as reported in Fig. 2. Third, the thermoluminescence glow curves were recorded after 1 and 2 flashes [49]. Fourth, the  $O_2$  evolution was measured under continuous saturating light conditions. The best conditions for the exchange were considered to be those under which the reversible inhibition of  $O_2$  evolution was the larger, the rate of the  $S_3Tyr_z^* + 2H_2O \rightarrow S_0Tyr_z + O_2$  the slower and the percentage of centers able to oscillate with a period of four the larger. Incubation for at least 6 h in the presence of 1 mM  $I^-$  were found to be these best conditions. The  $I^-$  concentration is lower than that used for the 3D X-ray structure [41] so that there is a possibility that the binding sites indentified in [41] which would correspond to the site with the lowest affinity for  $I^-$  remains empty in our conditions. Nevertheless, during the development of the protocol for the  $Cl^-/I^-$  exchange the iodide concentration was tested until 60 mM *i.e.* a value larger than that used for the 3D crystallography where the 2 sites have been shown to contain a iodide ion. With such a high concentration, although the miss parameter was much larger due to the secondary effects reported earlier, the rate of the  $S_3Tyr^*$  to  $S_0Tyr$  transition was similar to that reported with 1 mM  $I^-$ . Therefore, we can reasonably think that 1 mM  $I^-$  was enough for the halide exchange in the two sites provided that the duration of the incubation was at least 6 hours.

Oxygen evolving activity of purified PSII ( $5 \mu\text{g Chl mL}^{-1}$ ) was measured under continuous saturating white light at 25 °C by polarography using a Clark type oxygen electrode (Hansatech). A total of 0.5 mM dichloro-*p*-benzoquinone (PPBQ), dissolved in dimethyl sulfoxide, was added as an electron acceptor.

Cw-EPR spectra were recorded with a Bruker Elexsys 500 X-band spectrometer equipped for He-temperature with a standard ER 4102 (Bruker) X-band resonator, an Oxford Instruments cryostat (ESR 900) and an Oxford ITC504 temperature controller. Flash illumination at room temperature was provided by a Nd:YAG laser (532 nm, 550 mJ, 8 ns Spectra Physics GCR-230-10). PSII samples at  $\approx 1.1$ – $1.4 \text{ mg of Chl mL}^{-1}$  were loaded in the dark into quartz EPR tubes and dark-adapted for 1 h at room temperature. Then, the samples were synchronized in the  $S_1$ -state with one pre-flash [56]. After a further 1 h dark-adaptation at room temperature 0.5 mM PPBQ dissolved in ethanol 95% were added. Then, the samples were frozen to 198 K and then transferred to 77 K. The samples were degassed at 198 K prior to the recording of the spectra. Illumination at 198 K with a 1000 W tungsten-lamp filtered through water and infrared cut-off filters was done in a non-silvered Dewar in a  $CO_2$  ice-ethanol bath.

For time-resolved EPR measurements at room temperature, the spectrometer was equipped with a Super High Quality Bruker cavity. Saturating laser flash illumination at room temperature was provided by the laser described earlier. PSII at  $1.1 \text{ mg of Chl mL}^{-1}$  was loaded into a small volume flat cell (100  $\mu\text{L}$ ) in the presence of PPBQ, dissolved in dimethyl sulfoxide, and 1 mM potassium ferricyanide. Ferricyanide was added to avoid any contamination from the PPBQ  $\rightarrow$  signal which is detectable in the hundred  $\mu\text{s}$  time range after the flash illumination in the absence of ferricyanide. Formation and decay of the signal following laser flash illumination was measured at 32 magnetic field positions spread over 50 G and centered on the  $Tyr_z^*$  EPR signal. For each of the 32 magnetic field values, 16 scans were averaged. The two dimensional spectra (time *versus* field) of approximately 12 to 16 samples were averaged. Half of the 2D spectra

were obtained by increasing the magnetic field and the other half by decreasing the magnetic field.

Absorption changes were measured with a lab-built spectrophotometer [57] where the absorption changes are sampled at discrete times by short flashes. These flashes were provided by a neodymium:yttrium-aluminum garnet (Nd:YAG, 355 nm) pumped optical parametric oscillator, which produces monochromatic flashes (1 nm full-width at half-maximum) with a duration of 5 ns. Excitation was provided by a second neodymium:yttrium-aluminum garnet (Nd:YAG, 532 nm) pumped optical parametric oscillator, which produces monochromatic flashes at 700 nm (1 nm full-width at half-maximum) with a duration of 5 ns. The path length of the cuvette was 2.5 mm. PSII at  $25 \mu\text{g of Chl mL}^{-1}$  were dark-adapted for  $\approx 1$  h at room temperature (20–22 °C) before the additions of 0.1 mM PPBQ dissolved in dimethyl-sulfoxide.

### 3. Results

Optimization of the  $Cl^-/I^-$  exchange procedure in PSII from *T. elongatus* led us to set to 1 mM, for at least 6 h, the highest  $I^-$  concentration usable with minimal secondary effects such as those described earlier for high  $I^-$  concentrations. Routinely, the oxygen evolution activities of purified Ca/Cl-PSII and Sr/Cl-PSII were  $5000$ – $6000 \mu\text{mol } O_2 (\text{mg Chl})^{-1} \text{ h}^{-1}$  and  $1800$ – $2600 \mu\text{mol } O_2 (\text{mg Chl})^{-1} \text{ h}^{-1}$ , respectively [49]. Upon  $Cl^-/I^-$  exchange, the activities were  $\approx 70$ – $80\%$  of those prior to the exchange both in Ca-PSII and in Sr-PSII.

Fig. 1 shows the amplitude of the absorption changes associated with each flash in a series in Ca/Cl-PSII (black squares) and in Ca/I-PSII (red circles). Measurements were performed at 292 nm [49,58,59] and at 200 ms after the flashes, *i.e.* after completion of the reduction of  $Tyr_z^*$  by the water oxidizing complex. At this wavelength the reduction of PPBQ does not lead to any absorption changes and the successive oxidation steps of the water oxidizing complex have significant extinction coefficient [59]. The pattern, oscillating with a period of four, is clearly observed for both types of PSII preparations with very similar amplitude on the first flash. However, the damping is larger in Ca/I-PSII ( $\alpha \approx 0.1$ ) than in Ca/Cl-PSII ( $\alpha \approx 0.15$ ), assuming the same miss parameter on all S-state transitions.

To determine which step(s) is(are) kinetically affected and therefore responsible for the larger miss parameter in Ca/I-PSII we first measured the absorption changes at 292 nm in the 10  $\mu\text{s}$  to ms time ranges after the first three flashes in a series to assess the kinetics of

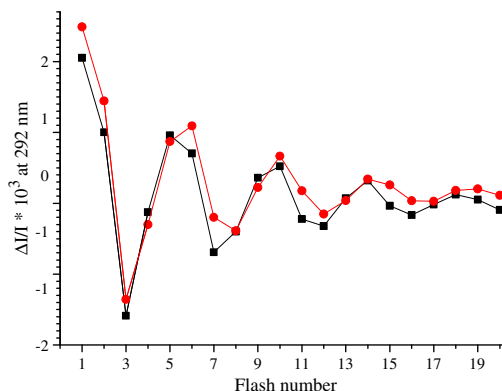


**Fig. 1.** Sequence of the amplitude of the absorption changes at 292 nm. The measurements were done during a series of saturating flashes (spaced 200 ms apart) given to dark-adapted Ca/Cl-PSII (black squares) or Ca/I-PSII (red circles). The samples ( $Chl = 25 \mu\text{g/mL}$ ) were dark-adapted for 1 h at room temperature before the addition of 100  $\mu\text{M}$  PPBQ. The measurements were done 200 ms after each flash. The buffers were glycerol 10%, betaine 1 M,  $CaCl_2$  15 mM,  $MgCl_2$  15 mM, Mes 40 mM, pH 6.5 for Ca/Cl-PSII and for Ca/I-PSII, glycerol 10%, betaine 1 M, NaI 1 mM,  $Ca(OH)_2$  15 mM,  $Mg(OH)_2$  15 mM, Mes 40 mM, pH 6.5 (adjusted with Mes powder). (For interpretation of the references to color in this figure legend, the reader is referred to the web version of this article.)

electron transfer associated with the  $S_1\text{Tyr}_Z^* \rightarrow S_2\text{Tyr}_Z$ ,  $S_2\text{Tyr}_Z^* \rightarrow S_3\text{Tyr}_Z$  and  $S_3\text{Tyr}_Z^* \rightarrow S_0\text{Tyr}_Z$  transitions in both the Ca/Cl-PSII and Ca/I-PSII. At 292 nm the absorption changes associated with the  $S_2\text{Tyr}_Z^* \rightarrow S_3\text{Tyr}_Z$  transition are small and preclude a reliable kinetic analysis. As shown in Fig. 2 we did not observe any significant differences for the kinetics of the absorption changes associated with the  $S_1\text{Tyr}_Z^* \rightarrow S_2\text{Tyr}_Z$  with a half time close to 50  $\mu\text{s}$  a value similar to that already reported in plant PSII [60] and *T. elongatus* PSII, here and [49]. In the  $S_3\text{Tyr}_Z^* \rightarrow S_0\text{Tyr}_Z$  transition, the decay of the  $\Delta I/I$  at 292 nm is biphasic [49,60]. The fast phase with a  $t_{1/2} \approx 50\text{--}100 \mu\text{s}$  in *T. elongatus* [49] and seen as a lag phase at 292 nm that has been interpreted as reflecting the electrostatically triggered expulsion of one proton from the catalytic center caused by the positive charge near/on  $\text{Tyr}_Z^*$ , e.g. [6,60–62]. The slow phase, seen as absorption decay with a  $t_{1/2} \approx 1.1 \text{ ms}$  in *T. elongatus* [49] corresponds to the  $S_0$  and  $\text{O}_2$  formations and to the release of an additional proton, e.g. [55,60–64]. Red curves of Fig. 2 shows that both the lag phase  $S_3\text{Tyr}_Z^* \rightarrow (S_3\text{Tyr}_Z^*)'$  with a  $t_{1/2} \approx 200\text{--}300 \mu\text{s}$  and the  $(S_3\text{Tyr}_Z^*)'$  to  $S_0\text{Tyr}_Z$  transition with a  $t_{1/2} \approx 6 \text{ ms}$  were markedly slowed down upon  $\text{Cl}^-/\text{I}^-$  exchange in Ca-PSII. Thus, the longer lifetime of the  $S_3\text{Tyr}_Z^*$  states likely contributes to the higher miss in Ca/I-PSII owing to a larger charge recombination probability. It should be noted that from the kinetics recorded after the 3rd flash in Ca/I-PSII (and Sr/I-PSII, see Fig. 6) there is no evidence for a fast  $\approx 1 \text{ ms}$  decay which argues against an incomplete  $\text{Cl}^-/\text{I}^-$  exchange.

Fig. 3 shows the EPR characteristics of the  $S_1$  and  $S_2$  states in the Ca/I-PSII sample. The spectra were recorded before (spectrum a, black) and after (spectrum b, red) illumination at 198 K. The difference spectrum “after-minus-before” the 198 K illumination is shown in blue (spectrum c). The spectrum recorded in the  $S_1$ -state exhibits signals at  $g = 7.4$  ( $\approx 920 \text{ G}$ ) and  $g = 5.8$  ( $\approx 1675 \text{ G}$ ), originating from the oxidized non-heme iron, e.g. [65–67]. The oxidized non-heme iron is mainly due to the presence of a significant amount of  $\text{Q}_B^-$  in the dark-adapted material [67] according to the reactions  $\text{Q}_B^- + \text{PPBQ} \rightarrow \text{Q}_B + \text{PPBQ}^{\cdot-}$  and then  $\text{Fe}^{\text{II}} + \text{PPBQ}^{\cdot-} + 2 \text{H}^+ \rightarrow \text{Fe}^{\text{III}} + \text{PPBQH}_2$ . The spectrum also features a narrow signal at  $g = 4.3$  ( $\approx 1580 \text{ G}$ ) and at  $g$  values  $\geq 5$  (between 500 and 1500 G) arising all from contaminants  $\text{Fe}^{\text{III}}$  (which should not be mistaken for the non-heme iron signal). The resonances at  $g \approx 3.0$  ( $\approx 2260 \text{ G}$ ),  $g \approx 2.2$  ( $\approx 3060 \text{ G}$ ) and  $g \approx 1.45$  ( $\approx 4695 \text{ G}$ ) correspond to the  $g_z$ ,  $g_y$  and  $g_x$ , respectively, of oxidized cytochrome(s). A careful examination of the  $g \approx 3.0$  signal (inset of Fig. 3) shows that it can be decomposed into two components. One arises, expectedly, from the  $\text{Cyt}_{c550}$  at  $g = 3.02$  [68,69], and another one which we ascribe to the oxidized  $\text{Cyt}_{b559}$  on the basis of the position of the shoulder at  $g = 3.08$  ( $\approx 2200 \text{ G}$ ), e.g. [70]. In Ca/Cl containing PSII, the  $\text{Cyt}_{b559}$  is mostly

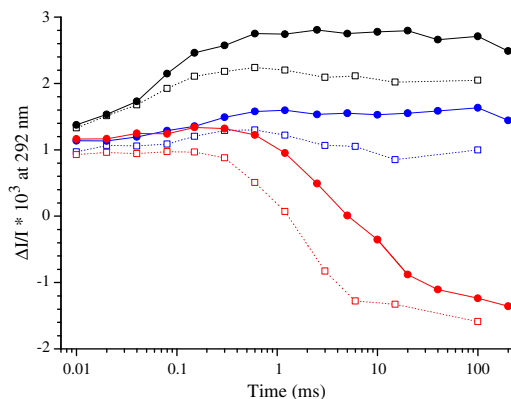


**Fig. 2.** Kinetics of the absorption changes at 292 nm after the first flash (black), the second flash (blue) and the third flash (red) given to dark-adapted Ca/Cl-PSII (open symbols, dashed lines) or Ca/I-PSII (close symbols, continuous line). Other experimental conditions were similar to those in Fig. 1. (For interpretation of the references to color in this figure legend, the reader is referred to the web version of this article.)

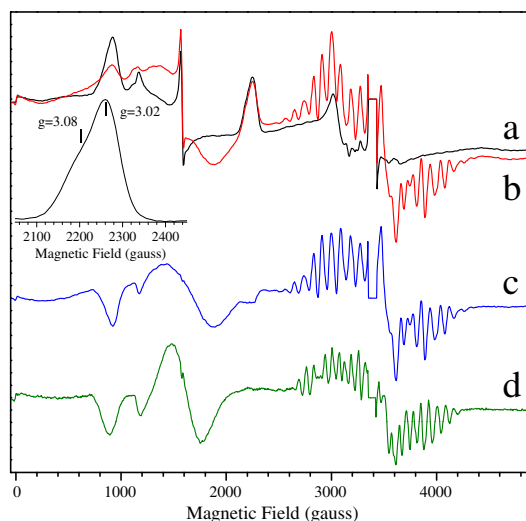


**Fig. 3.** Cw-EPR spectra recorded on Ca/I-PSII (a, b, c) and on Sr/I-PSII (d). The black spectrum (a) was recorded in the  $S_1$ -state and the red spectrum (b) after illumination at 198 K. The blue spectrum (c) is the red-minus-black difference spectrum. The green spectrum (d) is the red-minus-black difference spectrum recorded in Sr/I-PSII. Instrument settings: standard cavity; temperature, 8.6 K; modulation amplitude, 25 G; microwave power, 20 mW; microwave frequency, 9.3 GHz; modulation frequency, 100 kHz. The central part of the spectra corresponding to the  $\text{Tyr}_D^*$  region was deleted. In this experiment, PPBQ (50 mM) was dissolved in ethanol and used at 0.5 mM, final concentration. Inset:  $g_z$  signals from cytochromes. Instrument settings: temperature, 15 K; modulation amplitude, 25 G; microwave power, 5 mW. (For interpretation of the references to color in this figure legend, the reader is referred to the web version of this article.)

in its reduced state so that it is barely detectable by EPR. The clear detection of the  $g = 3.08$  signal means that the  $\text{Cl}^-/\text{I}^-$  exchange likely induced a decrease of the redox potential of  $\text{Cyt}_{b559}$  such that it is oxidized at the ambient potential. Upon illumination at 198 K, the characteristic  $S_2$  multiline signal was formed together with a broad signal at  $g = 4.05$  ( $\approx 1675 \text{ G}$ ). The  $S_2$  multiline signal is centered at  $g \approx 2$  and arises from the  $\text{Mn}_4\text{CaO}_5$  cluster in the  $\text{Mn}^{\text{IV}}_3\text{Mn}^{\text{III}}$  redox state with a spin state  $S = 1/2$  (see [54] and references therein for a recent discussion). Signals at  $g \approx 4$  also arise from the  $\text{Mn}_4\text{CaO}_5$  cluster in the  $\text{Mn}^{\text{IV}}_3\text{Mn}^{\text{III}}$  redox state but with a spin state  $S = 5/2$  [71]. The  $g = 4$  signal has been reported in plant PSII in various conditions, e.g. [72] and references therein, but in PSII from cyanobacteria never, to our knowledge, in such a large fraction of the centers as that found here. This is all the more noticeable as the present experiments were performed in the presence of ethanol, used as the solvent for PPBQ, which is known to favor the  $S = 1/2$  form at the expense of the  $S = 5/2$  form [73]. Moreover, the  $g$  value found here ( $g = 4.05$ ) was slightly lower than those generally found, i.e. between 4.15 and 4.25. Altogether, this suggests that, despite ethanol, the  $\text{Cl}^-/\text{I}^-$  exchange slightly modifies the environment of the  $\text{Mn}_4\text{CaO}_5$  cluster thereby promoting the  $S = 5/2$  form of the  $S_2$  state in the  $S_2$  state in PSII from *T. elongatus*. Finally, upon illumination at 198 K, the EPR spectrum displays the characteristic features resulting from the reduction of the non-heme iron, which takes place in the fraction of centers where it is oxidized prior to the illumination, and of the formation of the  $\text{Q}_A^-\text{Fe}^{\text{II}}$  signal at  $g = 1.94$  ( $\approx 3500 \text{ G}$ ), which occurs in the remaining fraction.

Spectrum d (green) in Fig. 3 is the difference spectrum “after-minus-before” the 198 K illumination in Sr/I PSII. We observed the multiline signal that is the signature of the  $S_2$  state and its pattern was slightly modified when compared to Ca-PSII as previously described [54,74]. In Sr/Cl-PSII, previous studies showed that in a fraction of PSII from the formation of the  $S_2$  state is not associated with the formation of a multiline spectrum but of a broad positive band with a peak at  $g = 5.25$  [75]. This particular band was not observed in the

Sr/I-PSII, but in a fraction of the centers formation of the  $S_2$  state was associated with a signal at  $g \approx 4$  ( $g = 4.15$  here). The  $g = 1.94$  band attests the formation of  $Q_A^- \text{Fe}^{\text{II}}$ .

We thus observed that, in both Ca-PSII and Sr-PSII, the  $\text{Cl}^-/\text{I}^-$  exchange favor the  $g \approx 4$  form. Similar observations have been reported with plant PSII [35], even though the extent to which the  $g \approx 4$  state was favored varied [32,35,36]. This variation likely stems from the protocols used for the  $\text{Cl}^-$ -depletion and the  $\text{I}^-$ -reconstitution.

According to the life time ( $t_{1/2} \approx 6$  ms) of the  $(S_3\text{Tyr}_Z^*)'$  state found here in the Ca/I-PSII (see Fig. 2), the decay of the  $(S_3\text{Tyr}_Z^*)'$  is long enough to allow for its detection by time-resolved EPR at room temperature. Fig. 4A shows a two dimensional spectrum (time versus field) recorded in Ca/I-PSII. Panel B shows two slices extracted from the 2D spectrum. The spectrum shown in black (Fig. 4B) has been extracted before the flash illumination and it corresponds to the  $\text{Tyr}_D^*$  spectrum. The spectrum shown in red (continuous line) has been extracted from the 2D spectrum immediately after the flash illumination and after subtraction of the baseline for each magnetic field value, i.e. after subtraction of the  $\text{Tyr}_D^*$  spectrum. It corresponds to the spectrum of  $\text{Tyr}_Z^*$ . The short lifetime of  $\text{Tyr}_Z^*$  in the lower S-states precludes its detection and it can thus only be detected in the  $(S_3\text{Tyr}_Z^*)'$

to  $S_0\text{Tyr}_Z$  transition. Thus the amplitude of the thereby obtained spectrum at most accounts for a fourth of the total  $\text{Tyr}_Z^*$  signal, and as expected multiplying this spectrum fourfold (red dashed line in Fig. 4B) yields a spectrum with an amplitude comparable to that of the  $\text{Tyr}_D^*$  spectrum.

This experiment was repeated with Sr/I-PSII and the results are shown in Fig. 5. Fig. 5B shows the spectra extracted from the individual kinetics shown in Fig. 5A after subtraction of the base line corresponding to the  $\text{Tyr}_D^*$  spectrum. This new 2D spectrum shows the spectra recorded from 1 ms to 200 ms after the flash. Fig. 5B shows that the decaying spectrum is that of the  $\text{Tyr}_Z^*$  species signal and that no change in the hyperfine structure of the signal occurred within the limit of the signal-to-noise ratio of the experiment.

Fig. 6 shows the absorption changes measured at 292 nm after the third flash and corresponding to the  $S_3\text{Tyr}_Z^* \rightarrow (S_3\text{Tyr}_Z^*)' \rightarrow S_0\text{Tyr}_Z$  transitions (symbols) together with the decay of the  $\text{Tyr}_Z^*$  signal measured by EPR (continuous lines) in the  $(S_3\text{Tyr}_Z^*)' \rightarrow S_0\text{Tyr}_Z$  transition in Ca/I-PSII (black) and Sr/I-PSII (red). For comparison purposes, the absorption and EPR data kinetics were normalized to the same amplitude and offset. Within experimental accuracy, the decays of the  $\text{Tyr}_Z^*$  EPR spectra matched perfectly the transient absorption changes. In

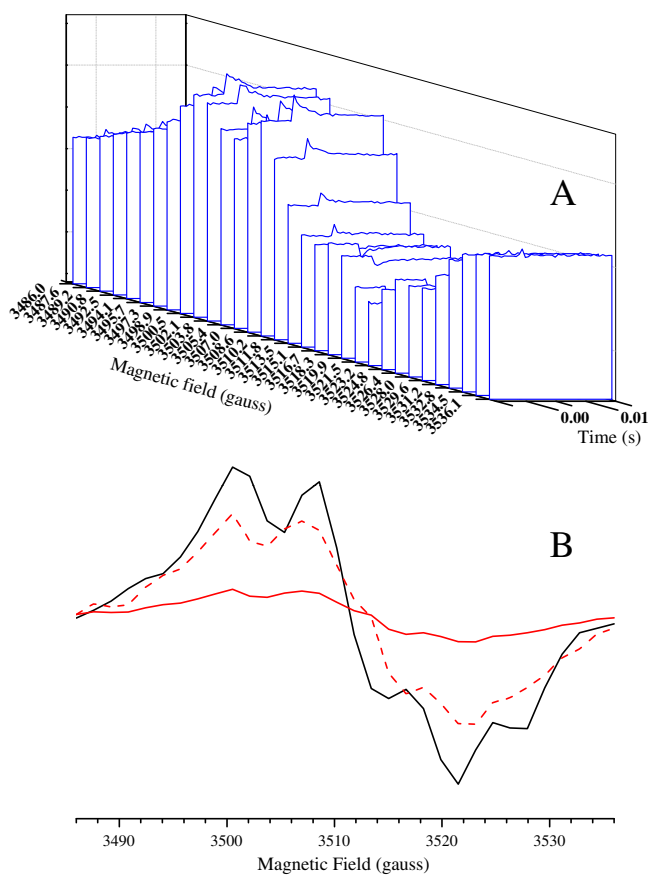


**Fig. 4.** Panel A: Formation and decay of the  $\text{Tyr}_Z^*$  signal following laser flash illumination of Ca/I-PSII measured at 32 magnetic field positions spread over 50 G from 3486 to 3536 G. For each of the 32 magnetic field values, 16 scans were averaged. The two dimensional spectra (time versus field) of approximately 12 to 16 samples were averaged. Half of the 2D spectra were obtained by increasing the magnetic field and the other half by decreasing the magnetic field. Other instrument settings; SHQ Bruker cavity; modulation amplitude, 4 G; microwave power, 20 mW; microwave frequency, 9.7 GHz; modulation frequency, 100 kHz and temperature, 293 K. The chlorophyll concentration was  $1.1 \text{ mg mL}^{-1}$ . Sampling time,  $500 \mu\text{s}$ . Panel B,  $\text{Tyr}_D^*$  (black) and  $\text{Tyr}_Z^*$  (red, continuous line) spectra extracted from the 2D spectrum in panel A. The  $\text{Tyr}_D^*$  spectrum is the envelope of the baseline before the flash and the  $\text{Tyr}_Z^*$  spectrum was obtained by extracting the first slice after the flash (i.e.  $\approx 1$  ms) after subtraction of the baseline before the flash which corresponds to the  $\text{Tyr}_D^*$  spectrum. The dashed line is the red continuous line times 4. (For interpretation of the references to color in this figure legend, the reader is referred to the web version of this article.)

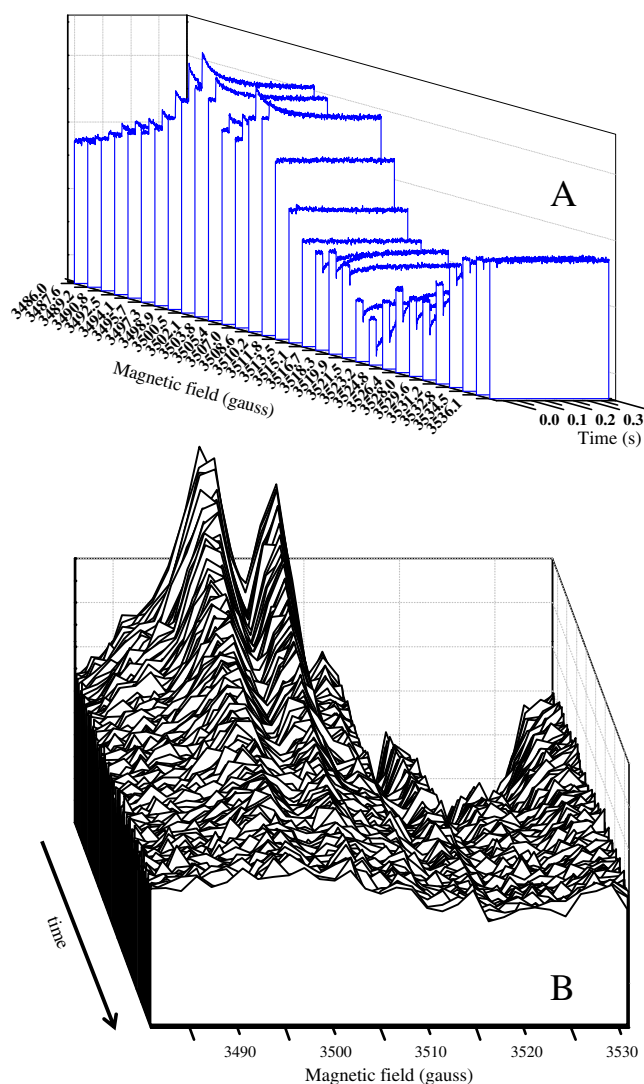


**Fig. 5.** Panel A: Formation and decay of the  $\text{Tyr}_Z^*$  signal following laser flash illumination of Sr/I-PSII measured at 32 magnetic field positions as in Fig. 4. Panel B:  $\text{Tyr}_Z^*$  spectrum from the data in Panel A obtained by subtraction of the  $\text{Tyr}_D^*$  spectrum versus time from 1 ms to 200 ms after the laser flash illumination. Same instruments settings as in Fig. 4.

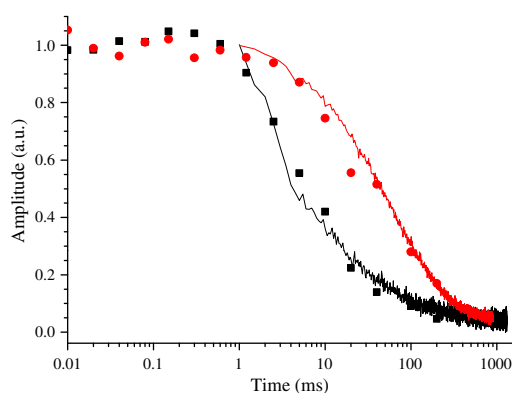


**Fig. 6.** Kinetics of the absorption changes at 292 nm after the third flash in Ca/I-PSII (black squares) and Sr/I-PSII (red circles). Measurements were done as described in Fig. 2. The continuous lines show the decay of the Tyr<sub>Z</sub><sup>•</sup> signal in Ca/I-PSII (black line) and Sr/I-PSII (red line). The EPR data correspond to the sum of the signal decay measured in Figs. 4 and 5 at 3500 and 3521.5 G, i.e. at magnetic field positions where the amplitude of the signal was the larger. (For interpretation of the references to color in this figure legend, the reader is referred to the web version of this article.)

Sr/I-PSII, the  $t_{1/2}$  of the lag phase  $S_3\text{Tyr}_Z^{\bullet}$  to  $(S_3\text{Tyr}_Z^{\bullet})'$  was difficult to estimate accurately but seemed longer than in Ca/I-PSII. The  $t_{1/2}$  of the  $(S_3\text{Tyr}_Z^{\bullet})'$  to  $S_0\text{Tyr}_Z$  transition was  $\approx 45$  ms in Sr/I-PSII.

The data aforementioned confirm that: *i*) the species decaying slowly and absorbing at 292 nm is the  $(S_3\text{Tyr}_Z^{\bullet})'$  state and *ii*) the reduction of Tyr<sub>Z</sub><sup>•</sup> is still the limiting step in the  $(S_3\text{Tyr}_Z^{\bullet})'$  to  $S_0\text{Tyr}_Z$  transition even in conditions where the  $t_{1/2}$  of this overall reaction was considerably slowed-down.

#### 4. Discussion

The effect of the Cl<sup>-</sup>/I<sup>-</sup> exchange on the O<sub>2</sub> activity in PSII isolated from *T. elongatus* is comparable to that in PSII from plant [33,34] in which it has been shown that chloride-depleted PSII supplemented with iodide sustained a high activity under saturating continuous illumination. Under flash illumination, the period four oscillations were also found only slightly more damped upon the Cl<sup>-</sup>/I<sup>-</sup> exchange, as already observed [33,34]. This increased miss parameter likely stems, at least partly, from the slower  $S_3\text{Tyr}_Z^{\bullet}$  to  $S_0\text{Tyr}_Z$  transition. However, this decreased rate only slightly affects the O<sub>2</sub> evolution in Ca/I-PSII. This is not unexpected since, according to the current understanding, the limiting step of the overall oxygen evolution *in vitro* is the exchange of the doubly reduced Q<sub>B</sub> molecule by an oxidized one. From an activity of 6000 μmol O<sub>2</sub> (mg Chl)<sup>-1</sup> h<sup>-1</sup>, in Ca/Cl-PSII [41] (i.e.  $\approx 50$  O<sub>2</sub> molecules per second), one can infer for the limiting step a lifetime of 20 ms, which corresponds to 2 Q<sub>B</sub>/Q<sub>B</sub>H<sub>2</sub> exchanges, a figure that is larger than the 6 ms lifetime found for the  $S_3\text{Tyr}_Z^{\bullet}$  to  $S_0\text{Tyr}_Z$  transition in Ca/I-PSII. In contrast to Ca/I-PSII, the sluggishness of the  $S_3\text{Tyr}_Z^{\bullet}$  to  $S_0\text{Tyr}_Z$  transition in Sr/I-PSII ( $t_{1/2} \approx 45$  ms) translates into a decreased the O<sub>2</sub> evolution activity.

We reported earlier that, in agreement with previous works e.g. [33,34,41], increasing the concentration of I<sup>-</sup> above 1 mM destabilizes the S<sub>2</sub> and S<sub>3</sub> states. We consider as unlikely the hypothesis according to which this would reflect the binding of I<sup>-</sup> to the third Cl<sup>-</sup> binding site identified by Umena et al. [3] because this site is located far apart the catalytic site. Rather this may reflect the reduction of the higher oxidation states of the cluster directly by I<sup>-</sup> that would make its way to the inner sanctum, possibly through the water conducting channel(s) now clearly identified [3,45]. Obviously, molecular dynamic simulations involving I<sup>-</sup>, the water channels and the amino acid residues constituting these channels would shed light on this issue.

In agreement with the most recent 3D structures, earlier enzymological studies have identified two binding sites for Cl<sup>-</sup> (see the

Introduction section). One of these, characterized by a larger affinity than the other, is strictly required for water splitting. The other one modulates the overall water oxidation activity. However, which among the two binding sites found in X-ray studies is the high affinity one remains to be identified. Guskov et al. [2] reported only one Cl<sup>-</sup>, which occupied one of the sites previously described in [40,41] – now referred to as Cl1 in [3] – pointing to this site as being the high affinity one. In addition to two water molecules, the Cl<sup>-</sup> in the Cl1 and Cl2 sites interact with two other side-chains provided by D2-Ly317 and D1-Glu333 for Cl1 and the backbone nitrogen of D1-Asn338 and CP43-Glu354 for Cl2. The Lys/Glu combination is likely to provide a stronger binding strength to the chloride than the Asn/Glu network [3].

In any case, identifying the high affinity binding site is only one step toward the understanding of the role of Cl<sup>-</sup>, located 7 Å apart from the catalytic center, in the mechanism of water oxidation. Cl<sup>-</sup> has been involved for long in the compensation reactions associated with deprotonation events, e.g. [21,23,32]. A recent study brought considerable support to this hypothesis [46]. Electrostatic calculations combined with molecular dynamic show that Cl<sup>-</sup> depletion induces the formation of a salt-bridge between D1-Asp61 and D2-Lys317, the two acido-basic side chains that contribute to the high affinity binding site discussed earlier. This salt bridge would modify the pKa of D1-Asp61, would interrupt a proton conducting network of H-bond and thus would prevent the efficient proton release associated with the accumulation of oxidizing power within the catalytic center [46]. The Cl1 site would thus set the conformation appropriate for the efficient conduction of protons. The involvement of D1-Asp61 has been nicely confirmed by the finding that, in site-directed mutants targeting this particular residue, the S<sub>3</sub> to S<sub>0</sub> transition and the accompanying oxygen release is dramatically decelerated upon the the Asp to Asn mutation [76–78]. The results presented here would be readily accounted for in this framework as the exchange of Cl<sup>-</sup> by I<sup>-</sup> would perturb the delicate proton conducting wire made of H-bonds, side chains and water molecules. It would thus leave unaffected the environment of Tyr<sub>Z</sub>, as shown by the unaltered EPR characteristic, but would slow down the release of (some) of the products of the water splitting process, protons. We note in addition, that the exchange of Cl<sup>-</sup> by I<sup>-</sup> has more specific functional consequences than the D1-Asp61Asn mutation. Indeed whereas the latter slows down not only the S<sub>3</sub> to S<sub>0</sub> transition but also those involving the lower S-states, the rate of the S<sub>1</sub> to S<sub>2</sub> transition was similar in the Ca/Cl- and Ca/I-PSII. Whereas this is expected if indeed Cl<sup>-</sup> determines the H<sup>+</sup> release since the S<sub>1</sub> to S<sub>2</sub> is associated with a stoichiometric proton release [79–81], it suggests that in the case of the D1-Asp61Asn mutant the structural consequences of the mutations propagates to the Mn<sub>4</sub>CaO<sub>5</sub> cluster likely via the two water molecules in coordination with the carboxylic group of D1-Asp61 on the one hand and acting as ligand to the cluster on the other hand. Thus, the picture emerging from these different studies is that, from a kinetic point of view, the release of product protons accompanying water splitting controls the overall reaction. Earlier studies of site directed mutants of D1-Asp61 came to a similar conclusion [76–78]. This has been rationalized in a model based on the notion that, owing to its small driving force, the oxidation of water was driven by the entropy change associated with the dilution of the products of its reaction. Since then, this model has been ruled out [82,83] and the kinetic control mentioned earlier would thus rely on different mechanistic rationales that remain to be unravelled.

DFT calculations [84] led to the conclusion that the presence of chloride in site 1 decreased by  $\approx 2$  kcal/mol (i.e.  $\approx 87$  mV) the limiting energy barrier between S<sub>3</sub> and S<sub>0</sub>, see [6,17] for recent discussions on the energetics of the S<sub>3</sub> to S<sub>0</sub> transition including the role of triggered proton transfers. Such a value is rather compatible with a

regulating role than to an essential role in the mechanism of O=O bond ascribed to the chloride ion in site 1. However, these DFT calculations were done without the knowledge of the number and coordinates of water molecules.

The  $\text{Ca}^{2+}/\text{Sr}^{2+}$  exchange increases the  $t_{1/2}$  of the  $\text{S}_3\text{Tyr}_Z^* \rightarrow \text{S}_0\text{Tyr}_Z$  transitions fourfold from 1.1 ms to 4.8 ms [49]. Here, we show that the  $\text{Cl}^-/\text{I}^-$  exchange results in an increase of this  $t_{1/2}$  from 1.1 ms to 6 ms in Ca-PSII, ( $a \approx 5$  fold increase), and from 4.8 ms to  $\approx 45$  ms in Sr-PSII, ( $a \approx 10$  fold increase). The two exchanges thus act synergistically which argues against the idea that they would affect distinct steps in a sequential process. Indeed, if such were the case, the rate of the overall process would be that of the slowest step and Sr/I-PSII would not differ so markedly from Ca/I-PSII or Sr/Cl-PSII. Crystallographic studies have shown however that  $\text{Ca}^{2+}$  and  $\text{Cl}^-$  are far apart and located on two opposite sides of the cluster [3]. In addition, Umena et al. [3] identified two main channels made of several water molecules in a row. One, hereafter named channel 1, has one of its extremities made by PsbV-Lys129 and the other is a network of water molecules around  $\text{Ca}^{2+}$ ,  $\text{Tyr}_Z$  and the Mn4 of the  $\text{Mn}_4\text{CaO}_5$  cluster. The other one, hereafter named channel 2, networks this Mn4 to a water chain involving side chains among which those from D1-Glu333, D1-Asp61 and D2-Lys317. Mn4 and its carboxylic ligand, D1-Glu333, may thus bridge these two water chains. Notably however, these two channels must fulfill different and specific functions. Indeed, the corollary of the framework according to which disrupting channel 2 considerably slows down or even blocks the proton release, is that there are no alternative efficient proton exit pathways, not even channel 1. Proton release would specifically occur along channel 2 and channel 1 would be responsible for the delivery of substrate water to the catalytic site. In any case, the present results suggest that either there is no efficient proton transfer from channel 2 to channel 1 or that channel 1 is a poor proton wire. Aquaporins do provide example of water chain with low conductance for proton. Yet these are rare cases that require a particularly tight control of the orientation of the water molecules to prevent the formation, even transiently, of a H-bond wire that would otherwise act as an efficient proton conducting chain (see [85] for a review on aquaporins). The current accuracy of the atomic structure does not allow assessing this model and this would require molecular dynamic simulations. The alternative possibility of the absence of efficient proton transfer between the two channels also translates into strong structural constraint. Indeed “proton sponges” in which proton exchange may occur via alternatives routes are often encountered as exemplified by the quinone binding site of bacterial reaction centers where multiple proton transfer pathways have been evidenced, e.g. [86].

The kinetic cross-talk between O=O bond formation on the one hand and proton release on the other hand is further illustrated by the comparison of the consequences of the  $\text{Ca}^{2+}/\text{Sr}^{2+}$  and  $\text{Cl}^-/\text{I}^-$  and the combined effects of the two. Experimentally, in the absence of crystals made with the different combinations for  $\text{Ca}^{2+}$ ,  $\text{Sr}^{2+}$ ,  $\text{Cl}^-$  and  $\text{Br}^-$  or  $\text{I}^-$ , this could be tested by comparing the Br-EXAFS in Ca/Br-PSII to that in Sr/Br-PSII (bromide is easier to detect than chloride e.g. [87]) and by comparing the Sr-EXAFS in Sr/Cl-PSII and Sr/Br-PSII.

It has been shown recently that upon the  $\text{Ca}^{2+}/\text{Sr}^{2+}$  exchange the slowing down of the  $\text{S}_3\text{Tyr}_Z^* \rightarrow \text{S}_0$  transition in Sr-PSII mainly arose from a decrease of the entropic part of the  $\Delta G^\ddagger$  of the reaction. This led us to propose that  $\text{Ca}^{2+}/\text{Sr}^{2+}$  exchange perturbs the distribution of the conformational microstates involving the water molecules bound to  $\text{Ca}^{2+}/\text{Sr}^{2+}$  and  $\text{Tyr}_Z$  and thereby hinders the overall water splitting process [55]. In addition, it has been proposed that the cluster of four water molecules involved in the  $\text{Mn}_4\text{Ca-Tyr}_Z$  motif also played an important role in the stabilization of the short hydrogen bond between the phenol group of  $\text{Tyr}_Z$  and the  $\text{N}_\epsilon$  of His190 in PSII [88] and that the rate constant of a proton coupled electron transfer from a tyrosine to an oxidant was strongly dependant on

the intra-molecular distance between the tyrosine and the base which accepts the proton, e.g. [89]. From all these data it is expected that a small change in the proton network around the  $\text{Mn}_4\text{Ca-Tyr}_Z$  motif would have an effect on the electron transfer reactions and on proton transfer reactions particularly for the two protons expelled during the  $\text{S}_3\text{Tyr}_Z^* \rightarrow \text{S}_0$  transition, e.g. [6,62,90,91] in addition to the references cited earlier for experimental evidences on the importance of the proton network. As pointed out in [3,45], D1-Glu333 is a ligand for both  $\text{Cl}_1$  and the 2 Mn (the Mn4 and Mn3) of the  $\text{Mn}_4\text{Ca}$  cluster. It thus seems likely that iodide, a weaker Lewis base than  $\text{Cl}^-$ , induces a weaker H-bonding with the closest water molecules and in a modification of the binding affinity of D1-Glu333 for the  $\text{Mn}_4\text{Ca}$  cluster.

The  $\text{Cl}^-/\text{I}^-$  exchange is also shown here to favor the spin  $S = 5/2$  state in the  $\text{S}_2$  state to the detriment of  $S = 1/2$  state. Interestingly, the experimental conditions that have been reported to favor the  $S = 5/2$  spin state usually relates to modification of the solvent properties (see [72] for a review). This suggests that the equilibrium between the two spin states depends on the H-bond network around the  $\text{Mn}_4\text{Ca}$  cluster, and the shift of the equilibrium upon Ca/Sr or Cl/I exchange would thus stem from the perturbation they induce in the H-bond network.

## 5. Conclusion

In both Ca-PSII and Sr-PSII the  $\text{Cl}^-/\text{I}^-$  exchange considerably slows down the two  $\text{S}_3\text{Tyr}_Z^* \rightarrow (\text{S}_3\text{Tyr}_Z^*)' \rightarrow \text{S}_0$  reactions in which the fast phase,  $\text{S}_3\text{Tyr}_Z^* \rightarrow (\text{S}_3\text{Tyr}_Z^*)'$ , reflects the electrostatically triggered expulsion of one proton from the catalytic center caused by the positive charge near/on  $\text{Tyr}_Z^*$  and the slow phase corresponds to the  $\text{S}_0$  and  $\text{O}_2$  formations and to a second proton release. The kinetic effects are interpreted by a model in which the  $\text{Ca}^{2+}$  binding site and the  $\text{Cl}^-$  binding site, although spatially distant, interact. This interaction is likely mediated by the H-bond and/or water molecules network(s) connecting the two sites that may participate to the release of the protons.

## Acknowledgements

MS was supported by JST-PRESTO program (4018) and Grant-in-Aid for scientific research from the Ministry of Education, Science, Sports, Culture and Technology (21612007). Ally Aukauloo and Aurélie Baron are acknowledged for discussions.

## References

- [1] K.N. Ferreira, T.M. Iverson, K. Maghlaoui, J. Barber, S. Iwata, Architecture of the photosynthetic oxygen-evolving center, *Science* 303 (2004) 1831–1838.
- [2] A. Guskov, J. Kern, A. Gabdulkhakov, M. Broser, A. Zouni, W. Saenger, Cyanobacterial photosystem II at 2.9-Å resolution and the role of quinones, lipids, channels and chloride, *Nat. Struct. Mol. Biol.* 16 (2009) 334–342.
- [3] Y. Umena, K. Kawakami, J.-R. Shen, N. Kamiya, Crystal structure of oxygen-evolving photosystem II at a resolution of 1.9 Å, *Nature* 473 (2011) 55–60.
- [4] B.A. Diner, F. Rappaport, Structure, dynamics, and energetics of the primary photochemistry of Photosystem II of oxygenic photosynthesis, *Annu. Rev. Plant Biol.* 53 (2002) 551–580.
- [5] G. Renger, Light induced oxidative water splitting in photosynthesis: energetics, kinetics and mechanism, *J. Photochem. Photobiol. B* 104 (2011) 35–43.
- [6] G. Renger, Mechanism of light induced water splitting in Photosystem II of oxygen evolving photosynthetic organisms, *Biochim. Biophys. Acta*, in press, doi:10.1016/j.bbabi.2012.02.005.
- [7] M.L. Groot, N.P. Pawlowicz, L.J. van Wilderen, J. Breton, I.H. van Stokkum, R. van Grondelle, Initial electron donor and acceptor in isolated Photosystem II reaction centers identified with femtosecond mid-IR spectroscopy, *Proc. Natl. Acad. Sci. U. S. A.* 102 (2005) 13087–13092.
- [8] A.R. Holzwarth, M.G. Muller, M. Reus, M. Nowaczyk, J. Sander, M. Rogner, Kinetics and mechanism of electron transfer in intact Photosystem II and in the isolated reaction center: pheophytin is the primary electron acceptor, *Proc. Natl. Acad. Sci. U. S. A.* 103 (2006) 6895–6900.
- [9] A.R. Crofts, C.A. Wraight, The electrochemical domain of photosynthesis, *Biochim. Biophys. Acta* 726 (1983) 149–185.
- [10] B.R. Velthuis, J. Ames, Charge accumulation at the reducing side of system 2 of photosynthesis, *Biochim. Biophys. Acta* 333 (1974) 85–94.

- [11] B. Kok, B. Forbush, M. McGloin, Cooperation of charges in photosynthetic O<sub>2</sub> evolution. I. A linear four step mechanism, *Photochem. Photobiol.* 11 (1970) 457–475.
- [12] P. Joliot, B. Kok, Oxygen evolution in photosynthesis, in: Govindjee (Ed.), *Bioenergetics of Photosynthesis*, Academic Press, New York, 1975, pp. 387–412.
- [13] F.M. Ho, S. Styring, Access channels and methanol binding site to the CaMn<sub>4</sub> cluster in Photosystem II based on solvent accessibility simulations, with implications for substrate water access, *Biochim. Biophys. Acta* 1777 (2008) 140–153.
- [14] J.W. Murray, J. Barber, Structural characteristics of channels and pathways in Photosystem II including the identification of an oxygen channel, *J. Struct. Biol.* 159 (2007) 228–237.
- [15] S. Vassiliev, P. Comte, A. Mahboob, D. Bruce, Tracking the flow of water through Photosystem II using molecular dynamics and streamline Tracing, *Biochemistry* 49 (2010) 1873–1881.
- [16] E.M. Sproviero, J.P. McEvoy, J.A. Gascon, G.W. Brudvig, V.S. Batista, Computational insights into the O<sub>2</sub>-evolving complex of Photosystem II, *Photosynth. Res.* 97 (2008) 91–114.
- [17] P.E.M. Siegbahn, Recent theoretical studies of water oxidation in Photosystem II, *J. Photochem. Photobiol. B* 104 (2011) 94–99.
- [18] S. Yamanaka, H. Isobe, K. Kanda, T. Saito, Y. Umena, K. Kawakami, J.-R. Shen, N. Kamiya, M. Okumura, H. Nakamura, K. Yamaguchi, Possible mechanisms for the O–O bond formation in oxygen evolution reaction at the CaMn<sub>4</sub>O<sub>5</sub>(H<sub>2</sub>O)<sub>4</sub> cluster of PSII refined to 1.9 angstrom X-ray resolution, *Chem. Phys. Lett.* 511 (2011) 138–145.
- [19] P.E.M. Siegbahn, The effect of backbone constraints: the case of water oxidation by the oxygen-evolving complex in PSII, *Chemphyschem* 12 (2011) 3274–3280.
- [20] S. Luber, I. Rivalta, Y. Umena, K. Kawakami, J.-R. Shen, N. Kamiya, G.W. Brudvig, V.S. Batista, S<sub>1</sub>-state model of the O<sub>2</sub>-evolving complex of Photosystem II, *Biochemistry* 50 (2011) 6308–6311.
- [21] F.C. Alnutt, E. Atta Asaf Adjei, R.A. Dilley, Chloroplast thylakoid proteins associated with sequestered proton-buffering domains – plastocyanin contributes buffering groups to localized proton domains, *J. Bioenerg. Biomembr.* 21 (1989) 535–551.
- [22] T.-A. Ono, J.-L. Zimmermann, Y. Inoue, A.W. Rutherford, Electron paramagnetic resonance evidence for a modified S-state transition in chloride-depleted Photosystem-II, *Biochim. Biophys. Acta* 851 (1986) 193–201.
- [23] A. Boussac, P. Sétif, A.W. Rutherford, Inhibition of Tyrosine Z photooxidation after formation of the S<sub>3</sub>-state in Ca<sup>2+</sup>-depleted and Cl<sup>-</sup>-depleted Photosystem-II, *Biochemistry* 31 (1992) 1224–1234.
- [24] K. Lindberg, T. Vänngård, L.-E. Andréasson, Studies of the slowly exchanging chloride in Photosystem-II of higher-plants, *Photosynth. Res.* 38 (1993) 401–408.
- [25] A. Boussac, Exchange of chloride by bromide in the manganese Photosystem II complex studied by cw- and pulsed-EPR, *Chem. Phys.* 194 (1995) 409–418.
- [26] P. van Vliet, A.W. Rutherford, Properties of the chloride-depleted oxygen-evolving complex of Photosystem II studied by electron paramagnetic resonance, *Biochemistry* 35 (1996) 1829–1839.
- [27] H. Wincencjusz, C.F. Yocum, H.J. van Gorkom, S-state dependence of chloride binding affinities and exchange dynamics in the intact and polypeptide-depleted O<sub>2</sub> evolving complex of Photosystem II, *Biochemistry* 37 (1998) 8595–8604.
- [28] K. Hasegawa, Y. Kimura, T.-A. Ono, Chloride cofactor in the photosynthetic oxygen-evolving complex studied by Fourier transform infrared spectroscopy, *Biochemistry* 41 (2002) 13839–13850.
- [29] P.H. Homann, Chloride and calcium in Photosystem II: from effects to enigma, *Photosynth. Res.* 73 (2002) 169–175.
- [30] J.P. McEvoy, G.W. Brudvig, Water-splitting chemistry of Photosystem II, *Phys. Chem. Chem. Phys.* 106 (2006) 4455–4483.
- [31] C.F. Yocum, The calcium and chloride requirements of the O<sub>2</sub> evolving complex, *Coord. Chem. Rev.* 252 (2008) 296–305.
- [32] K. Olesen, L.-E. Andréasson, The function of the chloride ion in photosynthetic oxygen evolution, *Biochemistry* 42 (2003) 2025–2035.
- [33] A. Rashid, P.H. Homann, Properties of iodide-activated photosynthetic water-oxidizing complexes, *Biochim. Biophys. Acta* 1101 (1992) 303–310.
- [34] H. Wincencjusz, C.F. Yocum, H.J. van Gorkom, Activating anions that replace Cl<sup>-</sup> in the O<sub>2</sub>-evolving complex of Photosystem II slow the kinetics of the terminal step in water oxidation and destabilize the S<sub>2</sub> and S<sub>3</sub> states, *Biochemistry* 38 (1999) 3719–3725.
- [35] P. van Vliet, Functional properties of the oxygen evolving complex of Photosystem II, PhD thesis (1996) Wageningen University, Netherlands.
- [36] D.I. Bryson, N. Doctor, R. Johnson, S. Baranov, A. Haddy, Characteristics of iodide activation and inhibition of oxygen evolution by Photosystem II, *Biochemistry* 44 (2005) 7354–7360.
- [37] G. Hind, H.Y. Nakatani, S. Izawa, Role of Cl<sup>-</sup> in photosynthesis. i. Cl<sup>-</sup> requirement of electron transport, *Biochim. Biophys. Acta* 172 (1969) 277–289.
- [38] S.M. Theg, P.H. Homann, Light-dependent, pH-dependent and uncoupler-dependent association of chloride with chloroplast thylakoids, *Biochim. Biophys. Acta* 679 (1982) 221–234.
- [39] T.-A. Ono, H. Nakayama, H. Gleiter, Y. Inoue, A. Kawamori, Modification of the properties of S<sub>2</sub> state in photosynthetic O<sub>2</sub>-evolving center by replacement of chloride with other anions, *Arch. Biochem. Biophys.* 256 (1987) 618–624.
- [40] J.W. Murray, K. Maghlaoui, J. Kargul, N. Ishida, T.-L. Lai, A.W. Rutherford, M. Sugiura, A. Boussac, J. Barber, X-ray crystallography identifies two chloride binding sites in the oxygen evolving centre of Photosystem II, *Energy Environ. Sci.* 1 (2008) 161–166.
- [41] K. Kawakami, Y. Umena, N. Kamiya, J.-R. Shen, Location of chloride and its possible functions in oxygen-evolving photosystem II revealed by X-ray crystallography, *Proc. Natl. Acad. Sci. U. S. A.* 106 (2009) 8567–8572.
- [42] A. Boussac, J.-L. Zimmermann, A.W. Rutherford, EPR signals from modified charge accumulation states of the oxygen evolving enzyme in Ca<sup>2+</sup>-deficient Photosystem-II, *Biochemistry* 28 (1989) 8984–8989.
- [43] X.S. Tang, D.W. Randall, D.A. Force, B.A. Diner, R.D. Britt, Manganese-tyrosine interaction in the Photosystem II oxygen-evolving complex, *J. Am. Chem. Soc.* 118 (1996) 7638–7639.
- [44] S. Un, A. Boussac, M. Sugiura, Characterization of the Tyrosine-Z radical and its environment in the spin-coupled S<sub>2</sub>TyrZ<sup>•</sup> state of Photosystem II from *Thermosynechococcus elongatus*, *Biochemistry* 46 (2007) 3138–3150.
- [45] K. Kawakami, Y. Umena, N. Kamiya, J.-R. Shen, Structure of the catalytic, inorganic core of oxygen-evolving Photosystem II at 1.9 angstrom resolution, *J. Photochem. Photobiol. B* 104 (2011) 9–18.
- [46] I. Rivalta, M. Amin, S. Luber, S. Vassiliev, R. Pokhrel, Y. Umena, K. Kawakami, J.-R. Shen, N. Kamiya, D. Bruce, G.W. Brudvig, M.R. Gunner, V.S. Batista, Structural-functional role of chloride in Photosystem II, *Biochemistry* 50 (2011) 6312–6315.
- [47] Y. Takahashi, S. Styring, A comparative-study of the reduction of electron-paramagnetic-resonance of signal-II slow by iodide and the iodo-labeling of the D2-protein in Photosystem-II, *FEBS Lett.* 223 (1987) 371–375.
- [48] M. Ikeuchi, H. Koike, Y. Inoue, Iodination of D1 (herbicide-binding protein) is coupled with photooxidation of I-125 (–) associated with Cl<sup>-</sup>-binding site in Photosystem-II water-oxidation system, *Biochim. Biophys. Acta* 932 (1988) 160–169.
- [49] N. Ishida, M. Sugiura, F. Rappaport, T.-L. Lai, A.W. Rutherford, A. Boussac, Biosynthetic exchange of bromide for chloride and strontium for calcium in the Photosystem II oxygen-evolving enzyme, *J. Biol. Chem.* 283 (2008) 13330–13340.
- [50] J. Kargul, K. Maghlaoui, J.W. Murray, Z. Deak, A. Boussac, A.W. Rutherford, I. Vass, J. Barber, Purification, crystallization and X-ray diffraction analyses of the *T. elongatus* PSII core dimer with strontium replacing calcium in the oxygen-evolving complex, *Biochim. Biophys. Acta* 1767 (2007) 404–413.
- [51] Y. Pushkar, J. Yano, K. Sauer, A. Boussac, V. Yachandra, Structural changes in the Mn<sub>4</sub>Ca cluster and the mechanism of photosynthetic water splitting, *Proc. Natl. Acad. Sci. U. S. A.* 105 (2008) 1879–1884.
- [52] M. Sugiura, A. Boussac, T. Noguchi, F. Rappaport, Influence of Histidine-198 of the D1 subunit on the properties of the primary electron donor, P680, of Photosystem II in *Thermosynechococcus elongatus*, *Biochim. Biophys. Acta* 1777 (2008) 331–342.
- [53] M. Sugiura, Y. Inoue, Highly purified thermo-stable oxygen-evolving photosystem II core complex from the thermophilic cyanobacterium *Synechococcus elongatus* having His-tagged CP43, *Plant Cell Physiol.* 40 (1999) 1219–1231.
- [54] N. Cox, L. Rapatskiy, J.-H. Su, D.A. Pantazis, M. Sugiura, L. Kulik, P. Dorlet, A.W. Rutherford, F. Neese, A. Boussac, W. Lubitz, J. Messinger, The effect of Ca<sup>2+</sup>/Sr<sup>2+</sup> substitution on the electronic structure of the oxygen-evolving complex of Photosystem II: a combined multi-frequency EPR, 55Mn-ENDOR and DFT study of the S<sub>2</sub> state, *J. Am. Chem. Soc.* 133 (2011) 3635–3648.
- [55] F. Rappaport, N. Ishida, M. Sugiura, A. Boussac, Ca<sup>2+</sup> determines the entropy changes associated with the formation of transition states during water oxidation by Photosystem II, *Energy Environ. Sci.* 4 (2011) 2520–2524.
- [56] S. Styring, A.W. Rutherford, In the oxygen-evolving complex of Photosystem II the S<sub>0</sub>-state is oxidized to the S<sub>1</sub>-state by D<sup>+</sup> (Signal-II slow), *Biochemistry* 26 (1987) 2401–2405.
- [57] D. Beal, F. Rappaport, P. Joliot, A new high-sensitivity 10-ns time-resolution spectrophotometric technique adapted to *in vivo* analysis of the photosynthetic apparatus, *Rev. Sci. Instrum.* 70 (1999) 202–207.
- [58] J. Lavergne, Absorption changes of Photosystem-II donors and acceptors in algal cells, *FEBS Lett.* 173 (1984) 9–14.
- [59] J. Lavergne, Improved UV-visible spectra of the S-transitions in the photosynthetic oxygen-evolving system, *Biochim. Biophys. Acta* 1060 (1991) 175–188.
- [60] F. Rappaport, M. Blanchard-Desce, J. Lavergne, Kinetics of electron-transfer and electrochromic change during the redox transitions of the photosynthetic oxygen-evolving complex, *Biochim. Biophys. Acta* 1184 (1994) 179–192.
- [61] M. Haumann, P. Liebisch, C. Muller, M. Barra, M. Grabolle, H. Dau, Photosynthetic O<sub>2</sub> formation tracked by time-resolved X-ray experiments, *Science* 310 (2005) 1019–1021.
- [62] L. Gerencser, H. Dau, Water oxidation by Photosystem II: H<sub>2</sub>O–D<sub>2</sub>O exchange and the influence of pH support formation of an intermediate by removal of a proton before dioxygen creation, *Biochemistry* 49 (2010) 10098–10106.
- [63] H. Koike, B. Hanssum, Y. Inoue, G. Renger, Temperature-dependence of S-state transition in a thermophilic cyanobacterium, *Synechococcus vulcanus* copeland measured by absorption changes in the ultraviolet region, *Biochim. Biophys. Acta* 893 (1987) 524–533.
- [64] M.R. Razeghifard, R. Pace, EPR kinetic studies of oxygen release in thylakoids and PSII membranes: a kinetic intermediate in the S<sub>3</sub> to S<sub>0</sub> transition, *Biochemistry* 38 (1999) 1252–1257.
- [65] J.-L. Zimmermann, A.W. Rutherford, Photoreductant-induced oxidation of Fe<sup>2+</sup> in the electron-acceptor complex of Photosystem II, *Biochim. Biophys. Acta* 851 (1986) 416–423.
- [66] V. Petrouleas, B.A. Diner, Light-induced oxidation of the acceptor-side Fe(II) of Photosystem-II by exogenous quinones acting through the QB binding-site.1. Quinones, kinetics and pH-dependence, *Biochim. Biophys. Acta* 893 (1987) 126–137.
- [67] A. Boussac, M. Sugiura, F. Rappaport, Probing the quinone binding site of Photosystem II from *Thermosynechococcus elongatus* containing either PsbA1 or PsbA3 as the D1 protein through the binding characteristics of herbicides, *Biochim. Biophys. Acta* 1807 (2010) 119–129.
- [68] C.A. Kerfeld, M.R. Sawaya, H. Bottin, K.T. Tran, M. Sugiura, D. Cascio, A. Desbois, T.O. Yeates, D. Kirilovsky, A. Boussac, Structural and EPR characterization of the soluble form of cytochrome c-550 and of the psbV2 gene product from the cyanobacterium *Thermosynechococcus elongatus*, *Plant Cell Physiol.* 44 (2003) 697–706.

- [69] M. Sugiura, S. Harada, T. Manabe, H. Hayashi, Y. Kashino, A. Boussac, Psb30 contributes to structurally stabilise the Photosystem II complex in the thermophilic cyanobacterium *Thermosynechococcus elongatus*, *Biochim. Biophys. Acta* 1797 (2010) 1546–1554.
- [70] M. Roncel, A. Boussac, J.L. Zurita, H. Bottin, M. Sugiura, D. Kirilovsky, J.-M. Ortega, Redox properties of the photosystem II cytochromes b559 and c550 in the cyanobacterium *Thermosynechococcus elongatus*, *J. Biol. Inorg. Chem.* 8 (2003) 206–216.
- [71] O. Horner, E. Rivière, G. Blondin, S. Un, A.W. Rutherford, J.-J. Girerd, A. Boussac, SQUID magnetization study of the infrared-induced spin transition in the S<sub>2</sub>-state of Photosystem II: Spin value associated with the g = 4.1 EPR signal, *J. Am. Chem. Soc.* 120 (1998) 7924–7928.
- [72] A. Boussac, A.W. Rutherford, Comparative study of the g = 4.1 EPR signals in the S<sub>2</sub>-state of Photosystem II, *Biochim. Biophys. Acta* 1457 (2000) 145–156.
- [73] J.-L. Zimmermann, A.W. Rutherford, Electron-paramagnetic resonance properties of the S<sub>2</sub> state of the oxygen-evolving complex of Photosystem-II, *Biochemistry* 25 (1986) 4609–4615.
- [74] A. Boussac, A.W. Rutherford, Nature of the inhibition of the oxygen-evolving enzyme of photosystem II induced by NaCl-washing and reversed by the addition of Ca<sup>2+</sup> or Sr<sup>2+</sup>, *Biochemistry* 27 (1988) 3476–3483.
- [75] A. Boussac, M. Sugiura, Y. Inoue, A.W. Rutherford, EPR study of the oxygen evolving complex in His-tagged Photosystem II from the cyanobacterium *Synechococcus elongatus*, *Biochemistry* 39 (2000) 13788–13799.
- [76] M. Hundelt, A.M.A. Hays, R.J. Debus, W. Junge, Oxygenic photosystem II: The mutation D1-D61N in *Synechocystis* sp. PCC 6803 retards S-state transitions without affecting electron transfer from Y<sub>2</sub> to P<sub>680</sub><sup>+</sup>, *Biochemistry* 37 (1998) 14450–14456.
- [77] P.L. Dilbeck, H.J. Hwang, I. Zaharieva, L. Gerencser, H. Dau, R.L. Burnap, The mutation D1-D61N in *Synechocystis* sp. PCC 6803 allows the observation of pH-sensitive intermediates in the formation and release of O<sub>2</sub> from Photosystem II, *Biochemistry* in press, DOI: [10.1021/bi201659f](https://doi.org/10.1021/bi201659f).
- [78] J. Clausen, R.J. Debus, W. Junge, Time-resolved oxygen production by PSII: chasing chemical intermediates, *Biochim. Biophys. Acta* 1655 (2004) 184–194.
- [79] P. Jahns, J. Lavergne, F. Rappaport, W. Junge, Stoichiometry of proton release during photosynthetic water oxidation – a reinterpretation of the responses of neutral red leads to a non integer pattern, *Biochim. Biophys. Acta* 1057 (1991) 313–319.
- [80] F. Rappaport, J. Lavergne, Proton release during successive oxidation steps of the photosynthetic water oxidation process – stoichiometries and pH-dependence, *Biochemistry* 30 (1991) 10004–10012.
- [81] H. Suzuki, M. Sugiura, T. Noguchi, Monitoring proton release during photosynthetic water oxidation in Photosystem II by means of isotope-edited infrared spectroscopy, *J. Am. Chem. Soc.* 131 (2009) 7849–7857.
- [82] M. Haumann, A. Grundmeier, I. Zaharieva, H. Dau, Photosynthetic water oxidation at elevated dioxygen partial pressure monitored by time-resolved X-ray absorption measurements, *Proc. Natl. Acad. Sci. U. S. A.* 105 (2008) 17384–17389.
- [83] D. Shevela, K. Beckmann, J. Clausen, W. Junge, J. Messinger, Membrane-inlet mass spectrometry reveals a high driving force for oxygen production by Photosystem II, *Proc. Natl. Acad. Sci. U. S. A.* 108 (2011) 3602–3607.
- [84] P.E.M. Siegbahn, Water oxidation in Photosystem II: oxygen release, proton release and the effect of chloride, *Dalton Trans.* 45 (2009) 10063–10068.
- [85] R.M. Stroud, D. Savage, L.J.W. Miercke, J.K. Lee, S. Khademi, W. Harries, Selectivity and conductance among the glycerol and water conducting aquaporin family of channels, *FEBS Lett.* 555 (2003) 79–84.
- [86] E. Nbedryk, J. Breton, M.Y. Okamura, M. Paddock, Identification of a novel protonation pattern for carboxylic acids upon Q<sub>B</sub> photoreduction in *Rhodospira rubra* sphaeroides reaction center mutants at Asp-L213 and Glu-L212 sites, *Biochemistry* 43 (2004) 7236–7243.
- [87] M. Haumann, M. Barra, P. Loja, S. Loscher, R. Krivanek, A. Grundmeier, L.-E. Andréasson, H. Dau, Bromide does not bind to the Mn<sub>4</sub>Ca complex in its S1 state in Cl<sup>-</sup>-depleted and Br<sup>-</sup>-reconstituted oxygen-evolving Photosystem II: evidence from X-ray absorption spectroscopy at the Br K-edge, *Biochemistry* 45 (2006) 13101–13107.
- [88] K. Saito, J.-R. Shen, T. Ishida, H. Ishikita, Short hydrogen bond between redox-active Tyrosine Y<sub>2</sub> and D1-His190 in the Photosystem II crystal structure, *Biochemistry* 50 (2011) 9836–9844.
- [89] M.-T. Zhang, T. Irebo, O. Johansson, L. Hammarström, Proton-coupled electron transfer from tyrosine: a strong rate dependence on intramolecular proton transfer distance, *J. Am. Chem. Soc.* 133 (2011) 13224–13227.
- [90] R.J. Service, W. Hillier, R.J. Debus, Evidence from FTIR difference spectroscopy of an extensive network of hydrogen bonds near the oxygen-evolving Mn<sub>4</sub>Ca cluster of Photosystem II involving D1-Glu65, D2-Glu312, and D1-Glu329, *Biochemistry* 49 (2010) 6655–6669.
- [91] T. Noguchi, M. Sugiura, FTIR detection of water reactions during the flash-induced S-state cycle of the photosynthetic water-oxidizing complex, *Biochemistry* 41 (2002) 15706–15712.